From the two-dimensional electron gas to antidot superlattices: magnetoresistance effects in the transition regime

1998 J. Phys.: Condens. Matter 10 3859

(http://iopscience.iop.org/0953-8984/10/17/016)

J. Phys.: Condens. Matter **10** (1998) 3859–3872. Printed in the UK PII: S0953-8984(98)89321-1

From the two-dimensional electron gas to antidot superlattices: magnetoresistance effects in the transition regime

O Steffens†, T Schlösser‡, P Rotter†, K Ensslin§, M Suhrke†, J P Kotthaus‡, U Rössler† and M Holland‖

† Institut für Theoretische Physik, Universität Regensburg, D-93040 Regensburg, Germany
‡ Sektion Physik, Ludwig-Maximilians-Universität, D-80539 München, Germany
§ Laboratorium für Festkörperphysik, ETH Zürich, CH-8093 Zürich, Switzerland
‖ Department of Electronics, University of Glasgow, Glasgow G12 8QQ, UK

Received 18 November 1997

Abstract. Magnetoresistance measurements and theoretical calculations for two-dimensional electron systems under a perpendicular magnetic field are presented which illuminate transport effects due to a periodic electrostatic potential modulation. We focus on features arising from the resolution of the magnetic miniband structure which are beyond the perturbative regime governed by the dispersion of Landau bands. Our non-perturbative quantum-mechanical calculations reveal that the dispersion of individual minibands is responsible for the complicated behaviour of the magnetoresistance in the regime of intermediate modulation strength. In particular, the interplay between miniband and scattering contributions to the conductivity leads to an almost structureless magnetoresistance in this regime followed by the formation of antidot peaks due to the miniband conductivity.

1. Introduction

Lateral superlattices superimposed on semiconductor heterostructures have revealed several phenomena that had not been predicted. Experimentalists and theorists have worked hand in hand to discover commensurability phenomena in the classical as well as in the quantum regime. A crucial parameter for all experiments is the ratio of the potential modulation V_0 to the Fermi energy E_F of the two-dimensional electron gas (2DEG)—in other words, whether the electrons have enough kinetic energy to overcome the artificially imposed potential pillars or not. In the regime of weak potential modulation, $V_0 \ll E_F$, Weiss oscillations [1, 2] dominate the magnetoresistance that can be explained classically by the guided centre drift of cyclotron orbits [3]. In terms of quantum mechanics, the dispersion of the Landau bands and the thus-arising group velocity lead to an additional conductivity mechanism, namely the Landau-band conductivity. For strong potential modulation, the dominant maxima of the magnetoresistance [4, 5] follow classically from the magnetic-field-induced regular parts in a predominantly chaotic phase space [6, 7]. In the quantum-mechanical picture, the strong potential modulation leads to a mixing of the Landau bands which split up into subbands. The spatial dispersion of these magnetic minibands is now the basis for the explanation of the observed magnetoresistance maxima [8–10]. While the classical description supplies intuitive pictures for the extreme modulation regimes in the framework of ballistic electron

0953-8984/98/173859+14$19.50

transport, it is not obvious how the intermediate regime, which is the focus of this paper, can be explained in classical terms.

At low temperatures, the classical commensurability oscillations have superimposed upon them semiclassical oscillations that can only be explained quantum mechanically. Features periodic in the magnetic field B (of Aharonov–Bohm type) and $1/B$ (of Shubnikov–de Haas type) were observed and were explained by the details of the respective potential landscape [11, 12]. Moreover, B-periodic oscillations arising from the quantum-mechanical band structure of a system with a periodic potential in a magnetic field were predicted for lateral superlattices with strong modulation potential and small lattice constant [13]. Quantum mechanics is crucial in order to understand these phase-coherence effects.

This paper focuses on a set of experiments where the amplitude of the potential modulation can be tuned over wide ranges via an applied gate voltage. The observations in the regime of intermediate modulation correspond neither to a monotonic increase of the amplitude of the Weiss oscillations predicted by classical calculations, nor even to oscillations of opposite phase governed by scattering between Landau bands as they follow from quantum-mechanical perturbation theory. Calculations based on the miniband structure arising in a magnetic field and using the concept of *miniband* conductivity reveal a better understanding of the experimental observations and even lead to predictions beyond what has been seen experimentally.

2. Experiments

In our samples, the 2DEG is realized by employing modulation-doped GaAs–(Ga_xAl_{1-x})As heterojunctions grown by molecular beam epitaxy. At $T = 4.2$ K the typical mobility in these samples is about 40 $m^2\ V^{-1}\ s^{-1}$, the carrier density n_s ranges from 3.0 to 5.2×10^{11} cm^{-2}. This corresponds to an elastic mean free path $L = 4.7\ \mu$m and to a Fermi wavelength λ_F of about 40 nm. The 2DEG is 38 nm beneath the crystal surface. It is necessary for the distance to be this small to obtain a steep and strong modulation potential.

The Hall-bar geometry is defined by wet chemical etching. The area between the voltage probes is 20 μm $\times$ 8 μm, which exceeds the scale of elastic and inelastic mean free paths. After creating a lattice of voids by using electron-beam lithography and an electron-sensitive resist layer (PMMA) on the sample surface, the latter is covered with an evaporated-metal gate (cf. figure 1). The proximity of this gate to the 2DEG now offers the unique possibility to induce a lateral superlattice potential, which is tunable over a wide range, while simultaneously realizing a lattice constant as small as 80 nm. Thus we were able to observe traces of the famous 'Hofstadter butterfly' [14] in the magnetoresistance as described in a previous publication [15, 16].

In this paper we will present magnetoresistance measurements for a system with the lattice constant $a = 215$ nm (see figure 1(b)) where the superlattice potential is continuously tuned from weak to strong modulation by changing the gate voltage from $+200$ meV to -750 meV. In the regime of weak modulation strength, electrons at the Fermi energy move classically along distorted, weakly perturbed cyclotron orbits (in the absence of an accelerating electric field). The opposite situation arises when the modulation amplitude is larger than the Fermi energy. Since the electrons are now classically excluded from certain 'islands' within the Fermi sea, this is called an *antidot* system.

Figure 2 gives a detailed account of the magnetoresistance properties at $T = 4.2$ K for the transition from one limit to the other. From top to bottom we distinguish three regimes that may be labelled as regions of strong, intermediate and weak-modulation strength. In the weak-modulation regime ($V_g = +200$ mV to -200 mV), the magnetoresistance ρ_{xx}

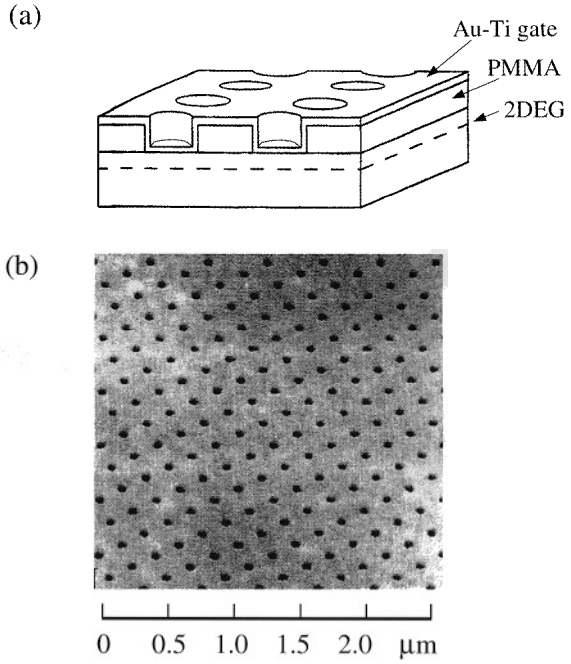

Figure 1. (a) A schematic sketch of a superlattice sample structure. By applying a voltage between the Au–Ti gates on the surface and the 2DEG, a periodic potential modulation is superimposed on the 2DEG. (b) An AFM image of the electron-sensitive resist layer with a lattice period of 215 nm.

shows two sets of $(1/B)$-periodic oscillations. At large magnetic fields there are the usual Shubnikov–de Haas (SdH) oscillations. At $T = 4.2$ K, they cannot be resolved below a magnetic field of $B = 0.75$ T, where their envelope, the second set of oscillations, becomes the predominant structure of ρ_{xx}. They are related to a commensurability of the superlattice constant and the electronic cyclotron diameter at the Fermi energy.

A larger negative gate voltage V_g corresponds to a stronger repulsion of the electrons beneath the voids in the sample—that is, to a stronger modulation amplitude. The enhanced repulsion leads to a reduced carrier density. In other words, a change in the Fermi energy intimately relates changes in the experimental potential modulation and the carrier density. This can be observed in a shift of the SdH oscillations.

The middle panel of figure 2 shows experimental magnetoresistance traces for an intermediate range of potential modulations. At magnetic fields $B > 1$ T, SdH oscillations are still visible. The amplitude of the commensurability oscillations has strongly decreased and they are no longer strictly $(1/B)$-periodic. Around $B = 0.9$ T, a pronounced maximum starts growing and in the regime of strong potential modulation (upper panel) develops into the feature that is generally related to an electron orbiting around a single antidot [17, 18]. Simultaneously, another maximum emerges at lower magnetic fields ($B = 0.2$ T) and develops into the usual antidot trace, being then identified with an electron trajectory at around four antidots. In its early phase of development, this maximum looks similar to features that were identified with magnetic breakdown for samples with a 1D modulation [19]. There are several features, such as the weak oscillations following the first maximum at around $B = 0.2$ T in the centre traces ($V_g = -400$ mV) that we cannot attribute to

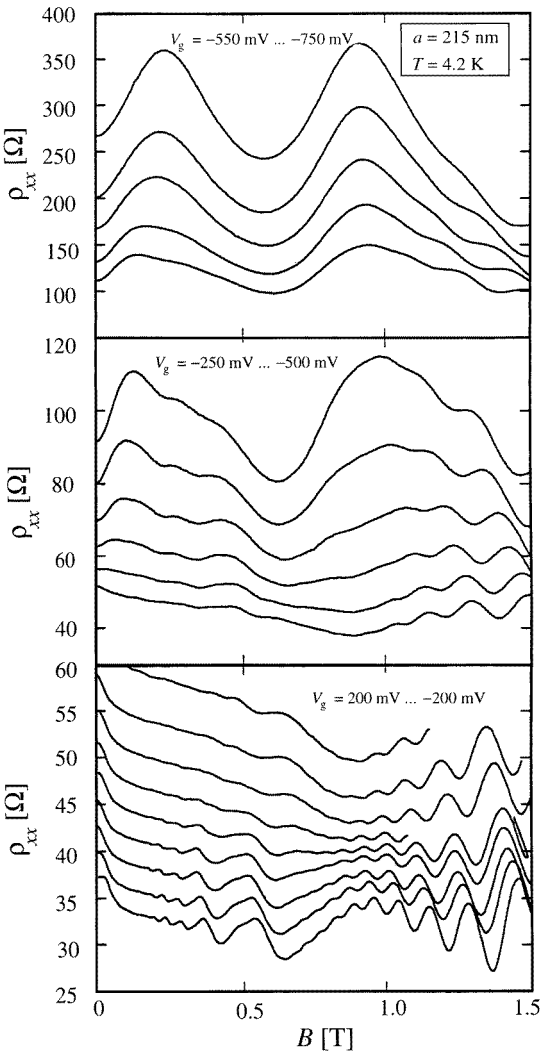

Figure 2. Experimental magnetoresistance traces for the transition from weak (bottom) to strong modulation (top), with $a = 215$ nm at $T = 4.2$ K. V_g is the applied voltage at the metal gate on the surface, changed in steps of 50 mV. From the Shubnikov–de Haas oscillations one determines a carrier density between 3.0 and 5.2×10^{11} cm^{-2}, which increases from top to bottom.

specific commensurability conditions. Furthermore, it is not at all obvious how the magnetic breakdown should develop into a feature that is related to pinned electron orbits. This is why numerical calculations as presented in the next section are absolutely crucial if we are to understand the regime of potential modulations that is not accessible to perturbative approaches.

The mobility in two-dimensional electron gases is known to be a monotonically growing function of the carrier density. The length of the elastic mean free path determines the maximum length for ballistic orbits that can play a role in lateral superlattices. Furthermore, there is a difference between the Drude mobility as deduced from the $B = 0$ resistance and quantum mobility that can be obtained from the amplitude of the SdH oscillations. There

is no simple notion of which mobility and, with it, which mean free path determines the strength of the commensurability features [20]. In the experiments, the mobility changes with carrier density and potential amplitude, both being tuned with the gate voltage. This interrelationship between the respective quantities makes it difficult to define the precise values for the calculation.

3. Theory

We describe the quantum-mechanical properties of two-dimensional (2D) electrons in the periodic lateral potential $V(x, y)$ and in a perpendicular magnetic field in the basis of the eigenstates of the corresponding single-particle effective-mass Hamiltonian. They can be classified by the magnetic wave vector $\boldsymbol{\Theta}$ and the miniband index n for integer and rational numbers n_Φ of flux quanta per unit cell of the lateral lattice [21]. For the scalar potential we use the phenomenological model

$$V(x, y) = V_0 \left[\cos\left(\frac{\pi}{a}x\right) \cos\left(\frac{\pi}{a}y\right) \right]^{2\alpha} \tag{1}$$

with lattice constant a. The theoretical results have been obtained for a typical value $a = 200$ nm which is close to the experimental one. The steepness of the potential can be adjusted by the parameter α and its strength is given by the amplitude V_0. The calculations have been carried out for a fixed value $\alpha = 4$ varying only V_0. Note that the transport properties are influenced by the potential shape as well [6, 10–12].

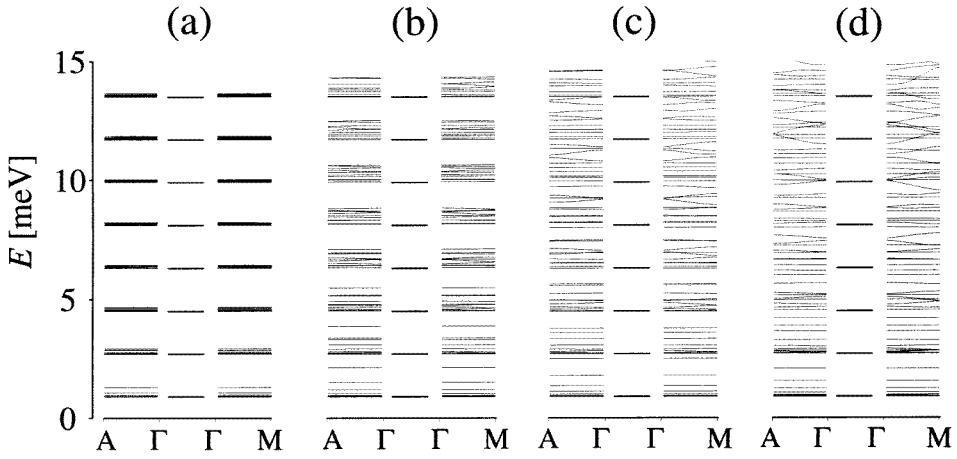

Figure 3. Magnetic miniband structure for $B = 1.034$ T ($n_\Phi = 10$) and different modulation amplitudes: (a) $V_0 = 1$ meV, (b) $V_0 = 5$ meV, (c) $V_0 = 10$ meV and (d) $V_0 = 20$ meV. For comparison, the ladders of the Landau levels for the unmodulated system, with $\hbar\omega_c = 1.80$ meV, are shown in the centres.

Figure 3 is an example of the resulting miniband structure when $n_\Phi = 10$. For different modulation amplitudes the dispersion $E_n(\boldsymbol{\Theta})$ is shown along the axis Γ–A in the [10] direction and Γ–M in the [11] direction within the first magnetic Brillouin zone. In the case of a small modulation amplitude (a), the degenerate Landau levels $E_{n_L} = \hbar\omega_c(n_L + \frac{1}{2})$ are split into ten almost dispersionless minibands, which are clustered around the positions of

the Landau levels. In general, if $n_\Phi = p/q$, one obtains p minibands from each Landau level. With increasing modulation strength V_0 the dispersion becomes more pronounced and the splitting grows. In the strong-modulation regime, $V_0 \gg \hbar\omega_c$ ((c) and (d)) one cannot associate each miniband with a particular Landau level because the Landau gaps are almost closed then. For $E < 2$ meV the kinetic energy of the electrons corresponds to a cyclotron radius R_c (or a spatial extent of their wavefunctions) of less than 40 nm, which is much smaller than the lattice constant $a = 200$ nm; the electrons are localized and the energy bands remain flat. But even for higher energies one finds flat minibands. The Fermi energy E_F lying in regions of flat or broad minibands does indeed play an important role for the transport properties of the system, since the dispersion of the latter gives rise to an additional contribution to the conductivity.

Within the regime of weak modulation, a perturbative treatment has been developed which ignores the coupling of different Landau levels [22]. In this approach, instead of using the miniband index n the eigenstates are labelled by the quantum numbers n_L and j, where j counts the subbands emerging from the n_Lth Landau level. When the splitting of the subbands which correspond to a particular Landau quantum number is so small that level broadening due to impurity scattering prevents a resolution of the individual subbands, one may regard each such group as a *Landau band* of oscillating width. Flat bands appear for

$$2R_c^{(n_L)} = a\left(\lambda - \frac{1}{4}\right) \qquad \lambda = 1, 2, \ldots \tag{2}$$

i.e. when the cyclotron diameter at the energy of the n_Lth Landau level satisfies a commensurability condition involving the lattice constant. In this case, the exact internal subband structure may be neglected in a *quasiclassical* calculation of the conductivity. The effect of higher harmonics of the modulation potential has also been investigated within this context [23].

In figure 4 the density of states $D(E)$ derived from the non-perturbative calculations is displayed for three different modulation amplitudes. The level broadening due to impurity scattering which we take into account in the self-consistent Born approximation (SCBA) [8, 9] smears out the details of the original density of states $N(E)$. The bandwidth oscillation with the Landau-level number n_L predicted by equation (2) can be seen from the envelope of the maxima of the broadened DOS for weak modulation (figure 4(a)). With increasing modulation amplitude one recognizes the breakdown of perturbation theory as the Landau gaps close (figures 4(b) and 4(c)). The emergence of extended states connected with the dispersion of *individual* minibands is, however, hidden in $D(E)$ and will be seen more clearly in the transport properties.

The diagonal and Hall conductivities are calculated in linear-response theory by means of the quantum Kubo formula [8, 9]. The diagonal components in units of e^2/h can be written as

$$\sigma_{\mu\mu}(E) = \frac{2\pi\ell^2}{n_\Phi}(\hbar\omega_c)^2 \sum_{n_1,n_2} \int \mathrm{d}^2\Theta \; \left|\langle n_1\boldsymbol{\Theta}|k_\mu|n_2\boldsymbol{\Theta}\rangle\right|^2 A_{n_1\Theta}(E) A_{n_2\Theta}(E) \tag{3}$$

which has to be convolved with the derivative of the Fermi function. This formula involves the impurity-averaged spectral functions $A_{n\Theta}(E)$ of the eigenstates $|n\boldsymbol{\Theta}\rangle$ and the matrix elements of the kinetic-momentum operator k_μ. The integral runs over the first magnetic Brillouin zone.

There are two different types of contribution to the diagonal conductivity. If $n_1 = n_2 = n$, the matrix element of k_μ is proportional to the group velocity of an electron in miniband n. It is connected with the miniband dispersion $E_n(\boldsymbol{\Theta})$ via the Hellmann–Feynman theorem.

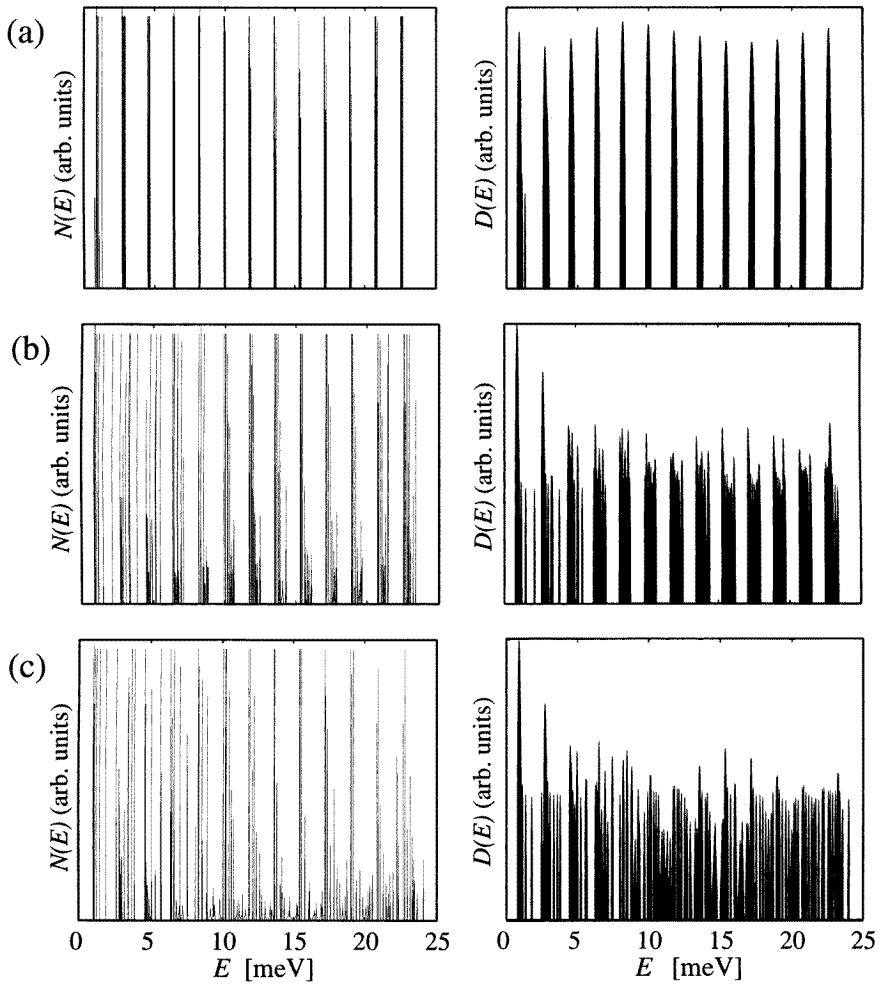

Figure 4. The density of states before (left-hand column) and after impurity broadening (right-hand column) for $B = 1.034$ T and different modulation amplitudes: (a) $V_0 = 1$ meV, (b) $V_0 = 5$ meV and (c) $V_0 = 10$ meV; the zero-field mobility is $\mu_e = 50\ m^2\ V^{-1}\ s^{-1}$ ($\tau = 20$ ps). Different scales are used for $N(E)$ and $D(E)$.

We call those contributions *miniband conductivity*. Strongly dispersive minibands give a large miniband conductivity whereas flat minibands give none at all. Notice that $[A_{n\Theta}(E)]^2$ is divergent without impurity scattering. The remaining part of $\sigma_{\mu\mu}$ consists of *scattering* contributions arising from the overlap of the spectral functions with different miniband indices ($n_1 \neq n_2$), analogous to the situation in the unmodulated 2DEG in a perpendicular magnetic field.

For weakly modulated systems with negligible Landau-level coupling, the authors of reference [22] obtained expressions for the conductivity components in leading order in V_0. They divided the longitudinal conductivity into two parts as well—namely, an *intra-Landau-band* (intra-LB) and an *inter-Landau-band* (inter-LB) contribution, according to whether $n_{L1} = n_{L2}$ or not. The spectral structure due to the oscillatory Landau-band width

modifies the conductivity as it is obtained from the unmodulated 2DEG. As long as the internal subband structure of a Landau band is not yet resolved due to impurity scattering, the intra-LB contribution increases with the Landau-band width and has minima for the flat-band conditions (2). At the same time, the inter-LB contribution which is essentially proportional to the square of the density of states $D(E)$ shows maxima. If the impurity scattering is weak enough, the intra-LB contribution determines the structure of the total conductivity. Once, however, with increasing modulation amplitude, the level broadening is no longer large enough to smear out the splitting of the Landau bands, it breaks down rapidly due to the reduced overlap of spectral functions with different subband indices j. For stronger impurity scattering, the inter-LB contribution is predominant even for the smallest modulation amplitudes. A very simple estimate based on the perturbation theory used in reference [22] suggests that the corrections to the conductivity of the unmodulated 2DEG, σ_0, are

$$\frac{\Delta\sigma_{xx}}{\sigma_0} \sim (1-\beta)\cos^2\left(2\pi\frac{R_c}{a}-\frac{\pi}{4}\right) \tag{4}$$

as long as the breakdown of the intra-LB contribution has not yet taken place. Here β depends on the scattering strength and is less than one for dominant intra-LB contribution and greater than one for dominant inter-LB contribution. Furthermore, β increases with carrier density and lattice constant (thus supporting inter-LB contributions), and its dependence on these parameters is also influenced by the potential shape, of course.

These dependencies have been found experimentally, too [24]. The scenario in the previous paragraph suggests that for sufficiently strong modulation the resistance should show maxima for the flat-band conditions irrespective of the modulation strength. This is, however, not the case. For higher modulation amplitudes, well beyond the perturbation regime, we find that the main transport properties originate from the increasing dispersion of the *individual* minibands. The analysis of the influence of this *miniband* conductivity is the central issue of our transport calculations.

In figure 5 the conductivity has been calculated from a fully quantum-mechanical, non-perturbative diagonalization for four modulation amplitudes from 1 to 20 meV using a temperature of $T = 4.2$ K, a carrier density of $n_s = 3.75 \times 10^{11}$ cm^{-2}, and a mobility $\mu_e = 50$ m^2 V^{-1} s^{-1} (i.e. $\tau = \tau_{tr} = 20$ ps). The resistance obtained from inversion of the conductivity tensor is given by $\rho_{xx} \approx \sigma_{xx}/\sigma_{xy}^2$ for $\sigma_{xx} = \sigma_{yy} \ll \sigma_{xy}^2$ ($\mu_e B \gg 1$). Therefore any oscillatory structure of the diagonal conductivity directly translates into the structure of the magnetoresistance as long as the Hall conductivity remains featureless beyond its Drude form. This can be seen in figures 5(b) and 5(d) for $B < 0.9$ T. The maxima in ρ_{xx} at $B \approx 0.55$ T and $B \approx 0.35$ T for $V_0 = 1$ meV are due to flat Landau bands with a high density of states which result in maxima of the inter-LB contribution. The latter is the only relevant mechanism for this small modulation strength at the chosen relaxation time. Arrows indicate two flat-band conditions predicted by equation (2). They agree nicely with the non-perturbative calculation. Slight deviations arising because of the higher harmonics of the modulation potential are expected [23].

For $V_0 = 5$ meV, additional maxima at $B \approx 0.65$ T and $B \approx 0.40$ T (marked by stars in figure 5(b)) appear between the flat-band conditions; they stem from high miniband dispersion at the Fermi energy, which leads to an enhanced miniband conductivity. Since individual minibands are already resolved (cf. figure 4(b)), the concept of Landau bands is no longer applicable. Despite an increased miniband conductivity, plotted as a dashed curve in figure 5(d), the total conductivity is smaller than for $V_0 = 1$ meV. The reason for this is that, for the parameters used in the calculation, the loss of scattering conductivity

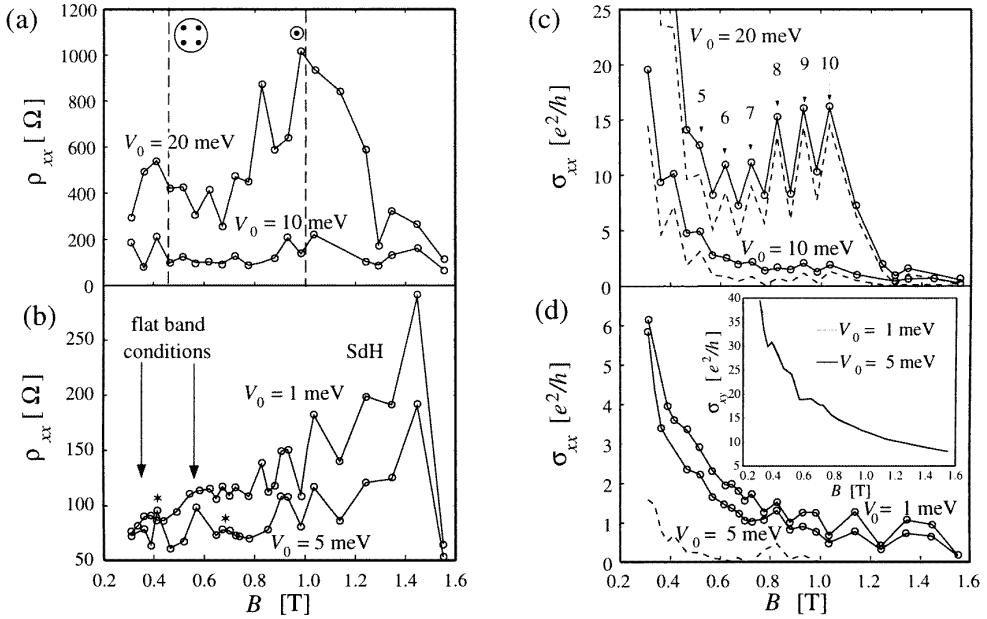

Figure 5. The magnetoresistance ρ_{xx} and diagonal conductivity σ_{xx} for different modulation amplitudes ($a = 200$ nm, $T = 4.2$ K, $n_s = 3.75 \times 10^{11}$ cm^{-2}, $\mu_e = 50$ m^2 V^{-1} s^{-1}): in the resistance plot (left-hand panel) the commensurate magnetic fields B_1 and B_4 mentioned in the text are marked by vertical dashed lines in (a). The stars in (b) indicate resistance peaks arising from enhanced miniband conductivity. The latter is shown as a dashed curve in the conductivity plot (right-hand panel) below the total conductivity (solid line). For $V_0 = 1$ meV (in (d)) the miniband conductivity is too small to be visible. The numbers above the arrows in (c) indicate the corresponding numbers of magnetic flux quanta per unit cell. The inset in (d) demonstrates the almost Drude-like behaviour of the Hall conductivity for $V_0 \leqslant 5$ meV.

which decreases because of the dispersion-related broadening of the density of states is not yet balanced by the gain from the miniband contribution.

When $V_0 > 5$ meV the miniband conductivity becomes the dominant part of the total conductivity and determines all of the details of its structure (cf. the dashed curves in figure 5(c)). For the interpretation of the resistance the influence of the Hall conductivity can no longer be assumed to be Drude-like [8, 9]. Its complicated structure contributes to the resistance maximum at around $B_1 = 1$ T, the traces of which can already be observed in σ_{xx} as the envelope of the finer oscillatory structures. The position of the maximum is in accordance with a commensurability between the lattice constant and the cyclotron diameter at the Fermi energy and can be interpreted in a simple classical picture as due to cyclotron orbits that fit around one antidot [17]. A second peak at around $B_4 = 0.44$ T corresponds to a cyclotron motion around a group of four antidots. These peaks are also present in the experiments of section 2. They are, however, shifted towards lower magnetic fields, which indicates a lower carrier density.

A striking feature of σ_{xx} consists in B-periodic oscillations that are superimposed on the classical peaks: their period corresponds to *exactly* one flux quantum per unit cell. Whenever n_Φ is an integer, the conductivity has a maximum. Since the effect originates in the miniband conductivity one expects to find the reason for this oscillation to be related to the miniband dispersion. Indeed, for rational n_Φ each Landau level splits into an increasing

number of minibands equal to the numerator of n_Φ with decreasing dispersion, as is already known from Hofstadter's butterfly [14]. This effect has been analysed in more detail in reference [13].

4. Discussion

In this section we will focus on the comparison between experimental and theoretical results. As already mentioned, the experimental carrier densities extracted from the SdH oscillations decrease with increasing potential modulation. Therefore we do not strive for a complete quantitative comparison and use a lattice constant of 200 nm together with some typical densities for the calculations. A small deviation from the experimental lattice constant does not affect the qualitative features of the magnetoresistance.

In the regime of very weak modulation strength we have carried out calculations in the perturbation scheme proposed in reference [22] but with much larger scattering time τ in order to demonstrate the conditions necessary to obtain dominant intra-LB conductivity. Therefore we not only ignore inter-Landau-level coupling in the band structure but also the quantum-mechanical effect that arises from a resolution of individual minibands (the breakdown of the intra-LB conductivity). As already mentioned before, this quasiclassical approximation is valid as long as the miniband splitting is small compared with the scattering broadening Γ [22].

The artificially high choice of τ in figure 6(c) (about one order of magnitude larger than in our non-perturbative calculations) provides the conditions that yield an intra-LB conductivity which is comparable to the inter-LB contribution. Accordingly, additional maxima appear between the flat-band positions, as a result of a high Landau-band dispersion at the Fermi energy. They increase in height with higher modulation amplitudes; one has to be aware, though, that the breakdown caused by the resolution of individual minibands is not included in these calculations. Comparison with the experimental resistance (figure 6(b)) shows that intra-LB conductivity is indeed responsible for the measured resistance structures at the smallest modulation strengths, with its pronounced maxima *between* the flat-band conditions.

How is this possible, given an electron mobility of less than 50 $m^2\ V^{-1}\ s^{-1}$? A realistic scattering mechanism with ionized impurities favours small-angle scattering. In this case the intra-LB conductivity is increased with respect to the inter-LB contribution. Making a quantitative statement, however, is difficult because the enhancement depends on the magnetic field, even for a given ratio of the transport relaxation time τ_{tr} and scattering lifetime τ at $B = 0$. This has been shown by a classical calculation of the amplitudes of Weiss oscillations in an anisotropic scattering model for a 1D modulation potential [20]. Since only one scattering time enters our theoretical concepts, one has to assume a much higher scattering time τ than in the experiment to account for a large τ_{tr} and hence the dominant intra-LB conductivity at the smallest modulation amplitudes.

For modulation amplitudes of 1 meV and 5 meV, we compare the exact calculations with the experiment in the weak-modulation regime. Figure 6(a) shows agreement of the positions of the resistance maxima and minima with the upper experimental curves in figure 6(b), where intra-LB conductivity has already broken down and inter-Landau-band scattering is dominant. With a carrier density of $5.0 \times 10^{11}\ cm^{-2}$, the miniband conductivity is still very small.

For $V_0 = 5$ meV, the latter already causes a little elevation in ρ_{xx} (arrow) at $B = 0.55$ T, which is located between two flat-band positions. The interplay of the two transport mechanisms results in an almost structureless experimental resistance when the

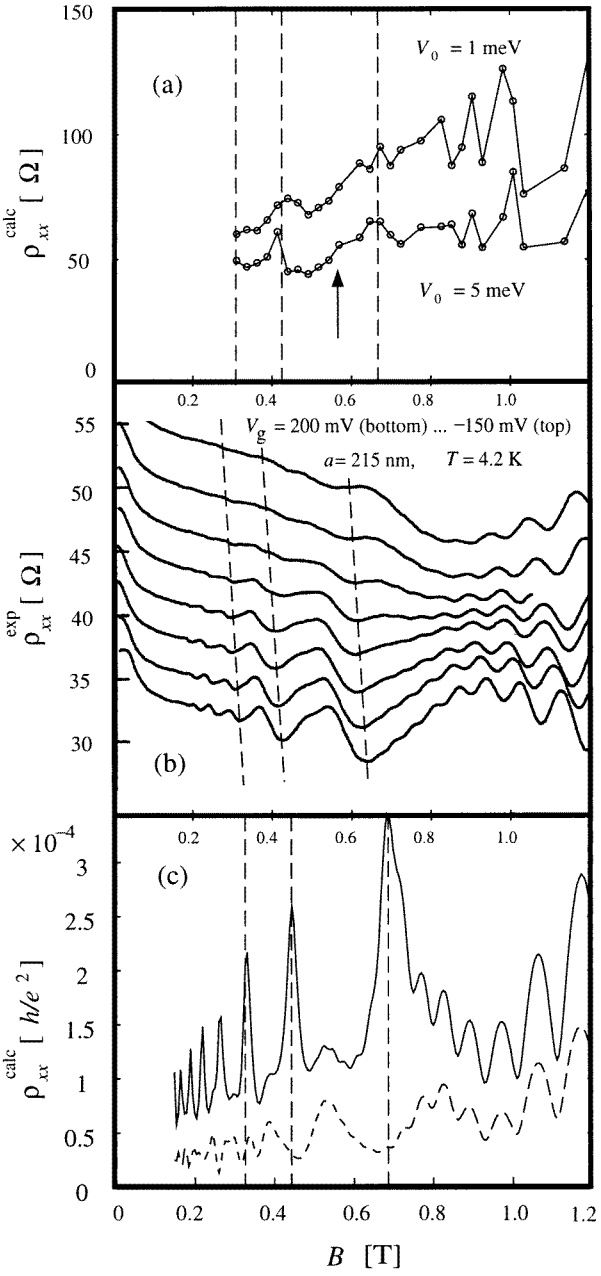

Figure 6. Comparison of experiment and theory for weak modulation at $T = 4.2$ K. (a) A fully quantum-mechanical calculation for two modulation amplitudes with $a = 200$ nm, $n_s = 5.0 \times 10^{11}$ cm^{-2} and $\mu_e = 50$ m^2 V^{-1} s^{-1} (assuming $\tau = \tau_{tr} \approx 20$ ps). The arrow marks a shoulder caused by the miniband conductivity. (b) The experiment with $n_s \approx (4.7–5.2) \times 10^{11}$ cm^{-2}. The carrier density decreases with increasing modulation strength (upward direction). (c) Quasiclassical perturbation theory (see the text) with $n_s = 5.4 \times 10^{11}$ cm^{-2} and $\tau = 200$ ps for $V_0 = 0.5$ meV. The dashed curve shows the resistance calculated with the intra-LB conductivity only, using the Drude result for the Hall conductivity to perform the tensor inversion. Vertical dashed lines indicate flat-band conditions derived from equation (2).

two contributions to the total conductivity are of the same magnitude.

The scenario following from the calculations coincides with measurements at lower temperatures ($T = 30$ mK) not shown here. The analysis of the envelopes of the SdH oscillations similar to that in reference [24] shows that the intra-LB contribution to the conductivity governs the resistance for the lowest modulation strengths whereas it has already broken down at a gate voltage of -100 mV leading to a dominating scattering contribution. The additional peaks emerging in the resistance for larger negative gate voltages at $B = 0.5$ T and at $B = 0.9$ T are connected with a clear decrease of the amplitude of the SdH oscillations in these field regions which indicates the increasing miniband conductivity.

The decrease of σ_{xx} (and ρ_{xx}) in the calculations between $V_0 = 1$ meV and $V_0 = 5$ meV is due to the reduction in the scattering conductivity when the dispersion of the minibands becomes larger. For sufficiently large modulation strength the miniband conductivity can compensate for that loss. The experiments show a similar feature which can be observed at $B = 0.9$ T where the resistance curves stay close together until miniband conductivity finally governs the resistance structure.

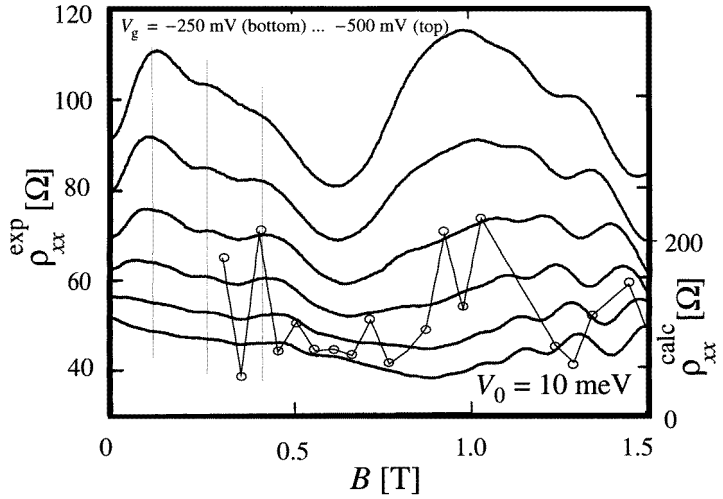

Figure 7. The experimental magnetoresistance for intermediate modulation strength with $a = 215$ nm and $T = 4.2$ K. The modulation strength increases in the upward direction. For comparison, the theoretical resistance curve for $V = 10$ meV, $n_s = 3.75 \times 10^{11}$ cm^{-2} and $a = 200$ nm is shown (with a different resistance scale). The vertical thin lines are guides to the eye.

For higher modulation amplitudes, miniband conductivity is the important transport mechanism. But since the influence of the Hall conductivity on resistance features can no longer be ignored, additional structures merge with those from the diagonal conductivity when ρ_{xx} is calculated by tensor inversion. The experimental resistances (see figure 7) show broad maxima in the region around 1 T and below 0.5 T. The position of the peak at around 1 T is near the commensurability condition for classical motion around one antidot; the other one corresponds to possible orbits around four antidots. Both maxima are reproduced in the calculation (with $V_0 = 10$ meV), but the B-periodic quantum oscillations with resistance maxima at integer n_Φ [13], which are visible in the theoretical traces, are not present in the experiment. Their amplitudes, which are much larger than the numerical inaccuracy in our

computations, depend on the scattering broadening of the energy levels. It is generally not easy to obtain a reliable value for the relevant parameter Γ since the relation between the transport relaxation time τ_{tr} and the scattering relaxation time τ is uncertain. Furthermore, the mobility in the sample (measured in zero magnetic field) changes with the gate voltage or the carrier density, respectively. As has been verified by various test calculations, the quantum oscillations are damped for larger scattering broadening. Increasing Γ by a factor of 10 reduces the oscillation amplitude by 80% (cf. also reference [13]). This, together with changes of the lattice constant over the macroscopic array which averages out the oscillations, is most probably the reason for the absence of flux-dependent quantum oscillations in the experiment.

The origin of the three maxima of the experimental resistance below 0.5 T is still unclear. Although they do not have the exact period of one flux quantum per unit cell, their regular structure might be a remnant of highly damped quantum oscillations in combination with the delicate structure brought about by the Hall conductivity.

5. Conclusion

We have measured the magnetoresistance of a two-dimensional electron gas with lateral potential modulation. By means of a tunable gate voltage, we have studied the transition from the weakly modulated 2DEG into the non-perturbative regime, which finally leads to an antidot system with the corresponding typical resistance features. The aim of the present work was to obtain some understanding of how the Weiss oscillations at very weak modulation amplitudes evolve into the classical commensurability peaks in the antidot regime. Our non-perturbative quantum-mechanical transport calculations allow an interpretation of the measurements and even suggest the existence of B-periodic resistance oscillations for intermediate modulation amplitudes which have not yet been observed in experiments. Although a direct comparison with experiments in this regime is difficult because the necessary parameters are not known explicitly, we find that all of the important features derive from the magnetic miniband structure. In particular, the growing influence of the miniband conductivity leads to additional magnetoresistance maxima between those arising from perturbative calculations. This results in an almost structureless magnetoresistance in the transition regime followed by the formation of the well-known antidot peaks.

Acknowledgments

The calculations were carried out on a Cray Y-MP supercomputer at the Leibniz Rechenzentrum in Munich. The authors would like to acknowledge financial support by the Deutsche Forschungsgemeinschaft (SFB 348).

References

[1] Weiss D, Zhang C, Gerhardts R R, von Klitzing K and Weimann G 1989 *Phys. Rev.* B **39** 13 020
[2] Winkler R W, Kotthaus J P and Ploog K 1989 *Phys. Rev. Lett.* **62** 1177
[3] Beenakker C W J 1989 *Phys. Rev. Lett.* **62** 2020
[4] Weiss D, Richter K, Vasiliadou E and Lütjering G 1994 *Surf. Sci.* **305** 408
[5] Schuster R and Ensslin K 1994 *Adv. Solid State Phys.* **34** 195
[6] Fleischmann R, Geisel T and Ketzmerick R 1992 *Phys. Rev. Lett.* **68** 1367
[7] Baskin É M, Gusev G M, Kvon Z D, Pogosov A G and Éntin M V 1992 *JETP Lett.* **55** 678

[8] Silberbauer H and Rössler U 1994 *Phys. Rev.* B **50** 11 911
[9] Silberbauer H, Rotter P, Suhrke M and Rössler U 1994 *Semicond. Sci. Technol.* **9** 1906
[10] Neudert R, Rotter P, Rössler U and Suhrke M 1997 *Phys. Rev.* B **55** 2242
[11] Weiss D, Richter K, Menschig A, Bergmann R, Schweizer H, von Klitzing K and Weimann G 1993 *Phys. Rev. Lett.* **70** 4118
[12] Schuster R, Ensslin K, Kotthaus J P, Böhm G and Klein W 1997 *Phys. Rev.* B **55** 2237
[13] Rotter P, Suhrke M and Rössler U 1996 *Phys. Rev.* B **54** 4452
[14] Hofstadter D R 1976 *Phys. Rev.* B **14** 2239
[15] Schlösser T, Ensslin K, Kotthaus J P and Holland M 1996 *Semicond. Sci. Technol.* **11** 1582
[16] Schlösser T, Ensslin K, Kotthaus J P and Holland M 1996 *Europhys. Lett.* **33** 683
[17] Weiss D, Roukes M L, Menschig A, Grambow P, von Klitzing K and Weimann G 1991 *Phys. Rev. Lett.* **66** 2790
[18] Lorke A, Kotthaus J P and Ploog K 1991 *Superlatt. Microstruct.* **9** 103
[19] Beton P H, Dellow M W, Main P C, Alves E S, Eaves L, Beaumont S P and Wilkinson C D W 1991 *Phys. Rev.* B **43** 9980
[20] Menne R and Gerhardts R R 1997 *Proc. 12th Int. Conf. on High Magnetic Fields in the Physics of Semiconductors II* ed G Landwehr and W Ossau (Singapore: World Scientific) p 323
[21] Silberbauer H 1992 *J. Phys.: Condens. Matter* **4** 7355
[22] Pfannkuche D and Gerhardts R R 1992 *Phys. Rev.* B **46** 12 606
[23] Gerhardts R R 1992 *Phys. Rev.* B **45** 3449
[24] Schlösser T, Ensslin K, Kotthaus J P and Holland M 1996 *Surf. Sci.* **361+362** 847